




RESEARCH ARTICLE | SEPTEMBER 18 2019

Efficient spin current generation in low-damping Mg(Al, Fe)₂O₄ thin films

Lauren J. Riddiford ; Jacob J. Wisser ; Satoru Emori ; Peng Li; Debangsu Roy; Egecan Cogulu; Olaf van 't Erve; Yong Deng; Shan X. Wang; Berend T. Jonker; Andrew D. Kent; Yuri Suzuki



Appl. Phys. Lett. 115, 122401 (2019)

<https://doi.org/10.1063/1.5119726>

 CHORUS



Articles You May Be Interested In

Ultrathin interfacial layer with suppressed room temperature magnetization in magnesium aluminum ferrite thin films

Appl. Phys. Lett. (September 2019)

Temperature dependence of Rashba-Edelstein magnetoresistance in Bi/Ag/CoFeB trilayer structures

Appl. Phys. Lett. (May 2017)

Orbital angular momentum contribution to angular dependent magnetoresistance in Tm₃Fe₅O₁₂/Pt/CuO_x films

Appl. Phys. Lett. (May 2024)

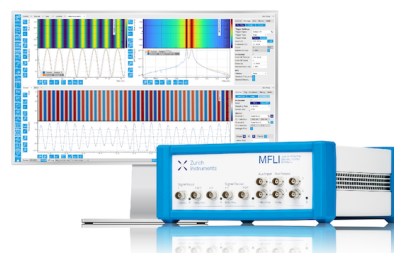
26 October 2024 18:36:47

Challenge us.

What are your needs for periodic signal detection?



[Find out more](#)



Efficient spin current generation in low-damping $\text{Mg}(\text{Al}, \text{Fe})_2\text{O}_4$ thin films

Cite as: Appl. Phys. Lett. **115**, 122401 (2019); doi: [10.1063/1.5119726](https://doi.org/10.1063/1.5119726)

Submitted: 11 July 2019 · Accepted: 14 August 2019 ·

Published Online: 18 September 2019






View Online



Export Citation



CrossMark

Lauren J. Riddiford,^{1,2,a)}  Jacob J. Wisser,^{1,2}  Satoru Emori,³  Peng Li,² Debangsu Roy,⁴ Egecan Cogulu,⁴ Olaf van 't Erve,⁵ Yong Deng,^{2,6} Shan X. Wang,^{2,6} Berend T. Jonker,⁵ Andrew D. Kent,⁴ and Yuri Suzuki^{1,2}

AFFILIATIONS

¹Department of Applied Physics, Stanford University, Stanford, California 94305, USA

²Ceballe Laboratory for Advanced Materials, Stanford University, Stanford, California 94305, USA

³Department of Physics, Virginia Tech, Blacksburg, Virginia 24061, USA

⁴Department of Physics, New York University, New York, New York 10003, USA

⁵Materials Science and Technology Division, Naval Research Laboratory, Washington, DC 45555, USA

⁶Department of Materials Science and Engineering, Stanford University, Stanford, California 94305, USA

a)lridd@stanford.edu

ABSTRACT

Low-damping magnetic insulators are essential for pure spin current-based electronics as they can generate and transfer spin currents without associated charge currents. Nanometer-thick epitaxial thin films of low-damping magnetic insulators are particularly important in order to control and switch the magnetization via spin transfer torques. We have recently developed films of the ferromagnetic insulator $\text{MgAl}_{0.5}\text{Fe}_{1.5}\text{O}_4$ (MAFO) with a low Gilbert damping parameter (~ 0.001). In contrast to $\text{Y}_3\text{Fe}_5\text{O}_{12}$ (YIG), MAFO films can be grown on a variety of substrates and have significant in-plane magnetic anisotropy, leading to higher spin-wave frequencies. Here, we demonstrate efficient spin current injection from MAFO into adjacent Pt and β -W layers by ferromagnetic resonance (FMR) broadening and inverse spin Hall effect measurements. Angular dependent magnetoresistance (ADMR) measurements indicate that the proximity effect magnetoresistance is small compared to the spin Hall magnetoresistance associated with spin pumping. FMR and ADMR measurements indicate that MAFO/Pt interfaces have a spin-mixing conductance of $\sim 2 \times 10^{14} \Omega^{-1} \text{m}^{-2}$, comparable to that of YIG/Pt. These measurements also show that the spin transport can be described by Dyakonov-Perel spin relaxation combined with an extrinsic spin Hall effect (from skew scattering). These results demonstrate the promise of spinel ferrites for spin current-based spintronics.

Published under license by AIP Publishing. <https://doi.org/10.1063/1.5119726>

Spintronics, based on the manipulation and transmission of spin, has attracted much attention as an avenue for alternative energy-efficient memory and electronics. The generation, transmission, detection, and control of pure spin currents (i.e., with no net charge current) have been studied in a range of material systems.^{1,2} Magnetic insulators have been identified as ideal spin current sources and media since these materials can generate and transmit pure spin currents with minimal dissipation from electron scattering. They also do not exhibit electrical current shunting which can complicate the interpretation of spin transport. Currently, the most commonly studied insulators for this purpose are iron garnets, particularly $\text{Y}_3\text{Fe}_5\text{O}_{12}$ (YIG) which has a Gilbert damping parameter ranging from 1 to 38×10^{-4} when grown on a single crystal $\text{Gd}_3\text{Ga}_5\text{O}_{12}$ (GGG).^{3–7} However, these materials require growth on paramagnetic GGG substrates and high deposition temperatures which limit their integration into the existing microelectronics. The

hexagonal ferrite $\text{BaFe}_{12}\text{O}_{19}$ has also been explored but has larger damping and the same processing challenges as garnets.^{8,9}

We have recently developed low damping insulating magnetic oxides with a spinel structure, specifically $\text{Ni}_{0.65}\text{Zn}_{0.35}\text{Al}_{0.8}\text{Fe}_{1.2}\text{O}_4$ (NZAFO) and $\text{MgAl}_{0.5}\text{Fe}_{1.5}\text{O}_4$ (MAFO).^{10–12} These spinel ferrites may be easily integrated with other spinel and perovskite oxides which, in turn, can be integrated with silicon.^{13,14} They also have higher effective magnetization than YIG, so the external field needed to excite a spin current is lower. We have already demonstrated efficient spin pumping in NZAFO/Pt bilayers and electrical detection of spin currents.¹² Since the magnetic damping of MAFO is 2–3 times lower than that of NZAFO, there is potential for even more efficient spin transfer.

In this paper, we demonstrate spin current generation in nanometer-thick MAFO films. By resonant excitation of the MAFO layer, we demonstrate significant spin pumping from MAFO films into

adjacent Pt and β -W layers through Gilbert damping enhancement and electrical voltage peaks that coincide with ferromagnetic resonance (FMR). The opposite signs in the transverse voltage signal in MAFO/Pt and MAFO/ β -W bilayers are consistent with the opposite signs of the spin Hall angle of Pt and β -W, indicating the electrical detection of spin currents from MAFO via the inverse spin Hall effect (ISHE). Angular dependent magnetoresistance (ADMR) measurements reveal that the spin Hall magnetoresistance (SHMR) is 10–25 times greater than the proximity-induced anisotropic magnetoresistance (AMR) contribution. From FMR and ADMR measurements, we find that Dyakonov-Perel (DP) spin relaxation¹⁵ and an extrinsic spin Hall effect (skew scattering) most consistently capture our results.¹⁶ We deduce a spin-mixing conductance of $\sim 2 \times 10^{14} \Omega^{-1} \text{ m}^{-2}$, indicating the transparency of the interface to spin currents. Finally, we observe a consistent spin diffusion length for Pt of around 2 nm between spin pumping and magnetotransport measurements, unlike YIG/Pt and Py/Pt systems which have reported spin diffusion lengths of Pt anywhere from 1.5 to 10 nm.¹⁷ Together these measurements indicate that MAFO films are excellent candidates for spin current-based heterostructures and devices.

We synthesized bilayer samples of $\text{MgAl}_{0.5}\text{Fe}_{1.5}\text{O}_4$ (MAFO) and Pt or β -W in order to probe spin pumping from nanometer-thick MAFO films into adjacent metallic layers. Epitaxial thin films of MAFO were deposited on the as-received (001)-oriented single crystal MgAl_2O_4 (MAO) substrates by pulsed laser deposition. A KrF 248 nm excimer laser, operating at a repetition rate of 1 Hz, was incident on a pressed stoichiometric target of $\text{MgAl}_{0.5}\text{Fe}_{1.5}\text{O}_4$ with a fluence of $\approx 2.1 \text{ J/cm}^2$. The depositions were performed at a substrate temperature of 450°C and a pressure of 10 mTorr of O_2 for a deposition rate of 0.011 nm/s . From our previous work, we found that 10–15 nm thick MAFO samples show the lowest damping and the highest crystalline quality with a typical rms roughness of 0.5 \AA .¹¹ Therefore, all samples were synthesized with 13 nm of MAFO. MAFO samples were removed from the chamber, and approximately one week later, platinum layers 1–20 nm thick were then sputtered at 150°C onto one set of MAFO samples. This was done in an Ar atmosphere of 3 mTorr and a dc power of 30 W. The growth rate during deposition was 0.036 nm/s . Atomic force microscopy shows that the rms roughness of Pt on MAFO is typically $\approx 1.2 \text{ \AA}$. 7 nm thick. β -W layers were sputtered at room temperature onto another set of MAFO samples in an Ar atmosphere of 3 mTorr and a dc power of 25 W, yielding a deposition rate of 0.042 nm/s . Due to the metastable β -phase of tungsten, we were limited to growing 7 nm of β -W on MAFO films.

The structural properties of MAFO were characterized with x-ray diffraction using a PANalytical X'Pert reflectometer. Reciprocal space mapping indicated that the MAFO layer was coherently strained to the underlying MAO substrate. Typical ω -rocking curves have a FWHM in the range of 0.045° – 0.06° , and Laue oscillations are observed, indicating excellent crystallinity.¹¹

Static magnetic properties were determined using a Quantum Design Evercool SQUID. Broadband FMR and inverse spin Hall effect measurements were carried out at room temperature with a broadband coplanar-waveguide-based spectrometer. For each measurement, the frequency is held fixed and the field is varied over 100 mT.¹⁰ For inverse spin Hall measurements, the metallic layer was patterned into a $500 \mu\text{m}$ Hall bar structure using photolithography and Ar ion milling, and the voltage was detected with a nanovoltmeter. ADMR measurements were

performed on patterned samples using a Quantum Design Dynacool System at room temperature.

MAFO films exhibited room-temperature saturation magnetization values of $100 \pm 7 \text{ kA/m}$ with $T_C \approx 400 \text{ K}$. We observed an in-plane easy [110] direction with coercive fields of $< 0.5 \text{ mT}$ and a harder [100] direction with typical saturation fields of $\sim 10 \text{ mT}$. The MAFO films had shape anisotropy which yields an out-of-plane anisotropy field of 0.12 T . However, strain anisotropy dominates in this material, leading to an overall out-of-plane anisotropy field of $\sim 1.5 \text{ T}$.¹¹

To probe dynamic properties and spin pumping in MAFO, we performed inverse spin Hall effect (ISHE) measurements to electrically detect spin pumping across MAFO/Pt and MAFO/ β -W interfaces. Resonant excitations in MAFO deposit spin angular momentum in the form of spin current into the adjacent metallic layer which is detected as the field derivative of the FMR absorption intensity dp/dH . This spin current gives rise to a transverse voltage in the heavy metal layer via the ISHE.¹⁸

For each frequency, the measured voltage peaks corresponded exactly to the FMR absorption field. Furthermore, the generated voltage changed the sign upon alternating the magnetic field direction (seen in Fig. 1). This indicates that the signal is unlikely to be from a proximity Nernst effect, which arises from a thermal gradient across the sample and in most cases does not change with a 180° rotation of the applied magnetic field.¹⁹ The spin Seebeck effect, which also creates a voltage due to a thermal gradient, cannot be eliminated but was shown to contribute minimally in YIG/Pt systems.¹⁹ The other potential source of a voltage signal is spin rectification, where oscillating magnetoresistance and microwave currents in the conducting layer yields a voltage. The origin of this is proximity-induced magnetism in the metal layer, which, Pt in particular, is susceptible according to the Stoner criterion.^{20,21}

In order to demonstrate that the observed transverse voltage is indeed dominated by the ISHE, we compared the sign of the transverse voltage measured across MAFO/Pt vs MAFO/ β -W samples. Figures 1(a) and 1(b) show opposite signs for the transverse voltage for the two types of samples, similar to what has been observed in Permalloy and YIG systems.^{5,18,22,23} Since the spin Hall angle θ_{SH} for Pt (0.0024–0.16) is opposite in sign to that of β -W (-0.14 to -0.33), MAFO/Pt and MAFO/ β -W should have opposite signs in transverse voltage if ISHE dominates.^{5,24} Other effects which would generate a

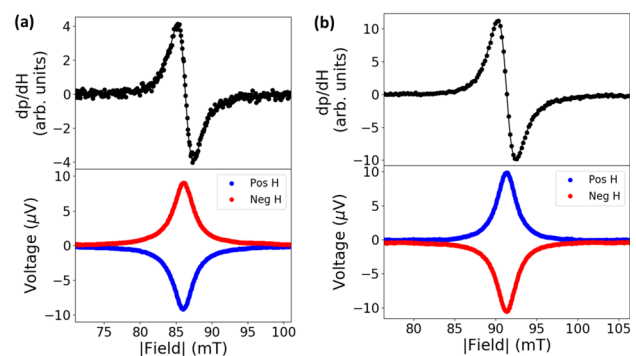


FIG. 1. FMR induced spin pumping and inverse spin Hall effect detection of the spin current at 10 GHz for (a) a bilayer with 2 nm Pt and (b) a bilayer with 7 nm β -W. These two samples are compared due to their almost identical resistance in the metallic layer.

voltage signal, such as spin rectification, do not depend on the spin Hall angle of the metal and thus would not show this sign difference.

To further elucidate the properties of spin transfer through the MAFO/metal interface, we performed FMR measurements on MAFO/Pt and MAFO/ β -W bilayers and compared them to single layer MAFO thin films. The magnetic loss in the single films and bilayers was measured by extracting the Gilbert damping parameter from the linear relationship between the resonance half-width-at-half-maximum linewidth ΔH and the excitation frequency f given by

$$\Delta H = \Delta H_0 + \frac{h}{g\mu_0\mu_B}\alpha f, \quad (1)$$

where the zero-frequency linewidth ΔH_0 is attributed to magnetic inhomogeneities.²⁵ The spectroscopic g-factor g was deduced to be 2.03 by fitting the frequency dependence of the resonant field.¹¹ When a heavy metal such as Pt or β -W is sputtered on the MAFO, an increase in the damping is observed [Fig. 2(a)]. The resonance field does not shift with the addition of the metal layer, indicating no change in MAFO's effective anisotropy. This increase in damping can be understood in terms of an additional contribution to the damping from spin pumping into the heavy metal so that the overall Gilbert damping of a magnetic material is given by $\alpha = \alpha_0 + \alpha^{SP}$, where α_0 is the intrinsic damping from the MAFO and α^{SP} can be modeled by

$$\alpha^{SP} = \frac{g\mu_B\hbar}{2e^2M_s t_{MAFO}} \left[\frac{1}{G_{\uparrow\downarrow}} + 2\rho_{NM}\lambda_s \coth\left(\frac{t_{NM}}{\lambda_s}\right) \right]^{-1}, \quad (2)$$

where t_{NM} , ρ_{NM} , and λ_s are the thickness, resistivity, and spin diffusion length of the metallic layer, respectively. M_s is the saturation magnetization of MAFO, and $G_{\uparrow\downarrow}$ is the spin mixing conductance.^{24,26,27}

In Fig. 2(b), an increase in damping was observed with increasing Pt thickness which saturates to a nearly constant value by 5 nm. This increase in damping is attributed to spin current flowing from the MAFO layer into the Pt layer. A significant damping increase was also seen in MAFO/ β -W bilayers. As a control, MAFO/Cu bilayers were also synthesized, and their Gilbert damping parameters were measured. Due to the weak spin-orbit coupling and long spin diffusion length of Cu, we would predict no significant enhancement of damping with the addition of Cu. As expected, we measure the increase to be only 10% above that of α_0 .

By fitting the Pt data in Fig. 2(b) to Eq. 2, we extracted the spin mixing conductance $G_{\uparrow\downarrow}$ at the interface, along with the spin diffusion length

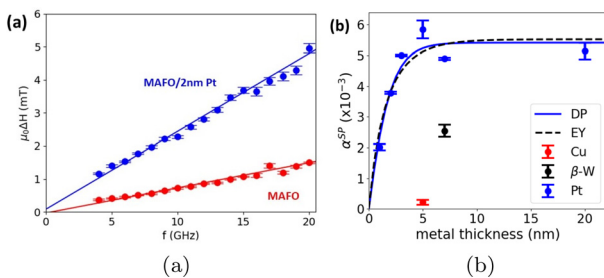


FIG. 2. (a) In-plane FMR linewidth vs excitation frequency for a 13 nm MAFO sample and for the same sample with 2 nm Pt. (b) The change in Gilbert damping ($\alpha^{SP} = \alpha - \alpha_0$) for different thicknesses of metals sputtered on 13 nm MAFO. The blue line is a fit of the MAFO/Pt data to Eq. (2) for the Dyakonov-Perel mechanism and the Elliott-Yafet mechanism.

λ_s of Pt. Here, the resistivity of Pt was measured for each thickness and fit to the empirical model $\rho(t) = \rho_{bulk} + \rho_i \exp(-t/L)$. We find $\rho_{bulk} = 1.9 \times 10^{-7} \Omega \text{ m}$, $\rho_i = 5.9 \times 10^{-7} \Omega \text{ m}$, and $L = 3.2 \text{ nm}$. Both the Dyakonov-Perel (DP) mechanism (with a constant spin diffusion length) and the Elliott-Yafet (EY) mechanism (with a resistivity-dependent spin diffusion length) fit these data equally well.¹⁵ With the DP mechanism (which we later show best fits the ADMR results), we obtained a spin mixing conductance of $G_{\uparrow\downarrow} = (2.1 \pm 0.2) \times 10^{14} \Omega^{-1} \text{ m}^{-2}$ and the spin diffusion length to be $\lambda_s = 2.0 \pm 0.4 \text{ nm}$, which is within the reported range of typical values for bilayers with Pt.^{24,28,29} The spin mixing conductance is on the higher end of typical values in the literature for YIG/Pt systems $(0.6-4) \times 10^{14} \Omega^{-1} \text{ m}^{-2}$, suggesting efficient spin pumping in MAFO/Pt bilayers.^{4,5,24,29} However, interfacial spin scattering,^{30,31} the effect of proximity induced magnetism in the metallic layer,³² or radiative damping could also contribute to increased Gilbert damping.³³ Thus, these results of enhanced Gilbert damping alone cannot conclusively quantify spin pumping.

We performed ADMR measurements in order to determine the relative contributions of SHMR, due to the transfer of spin angular momentum across the interface, and proximity-induced AMR to the overall magnetoresistance. These two sources of magnetoresistance can be disentangled by rotating the magnetization in planes perpendicular to the sample.^{34,35} When the magnetic field is rotated with respect to the current direction [see Fig. 3(a)], the only contribution to magnetoresistance is the AMR resulting from the moments of the Pt coupling to the moments of MAFO. However, when the magnetic field is rotated orthogonal to the current direction [see Fig. 3(c)], the only contribution is from SHMR. This is due to a difference in conductivity depending on whether a spin current generated in the metal layer can be absorbed by the magnetic layer or is reflected.²⁴

Due to the strain-induced easy plane anisotropy of the MAFO films, fields above the effective saturation field of 1.5 T are required to see the full ADMR effects. However, there is a quadratic dependence of magnetoresistance on the magnetic field at very large fields due to the Hanle magnetoresistance.³⁶ Thus, the ADMR for all samples was measured at 2 T, which is strong enough to saturate the MAFO magnetization in any direction but weak enough that any contribution from the Hanle magnetoresistance was minimal. The SHMR and AMR for 2 nm Pt, for example, are shown in Figs. 3(b) and 3(d). The ADMR deviates from a $\cos^2 \theta$ dependence due to the discrepancy between the angle of the applied field and the angle of the magnetization in MAFO. The fit curves in Figs. 3(b) and 3(d) were calculated through a free energy minimization procedure detailed further in Ref. 12. For both MAFO/Pt and MAFO/ β -W, the AMR magnitude is very small (around $1-1.5 \times 10^{-5}$) times larger for 2 nm Pt and ~ 10 times larger for β -W. This indicates that induced magnetism in the metal layer is minimal and that spin pumping effects dominate the magnetization dynamics of the bilayers.

We also analyzed the Pt thickness dependence of the SHMR to estimate the spin mixing conductance as described in Ref. 37

$$\left| \frac{\Delta\rho_{SHMR}}{\rho_0} \right| = \frac{\theta_{SH}^2 (2\lambda_s^2 \rho_{Pt}) t_{Pt}^{-1} G_{\uparrow\downarrow} \tanh^2\left(\frac{t_{Pt}}{2\lambda_s}\right)}{1 + 2\lambda_s \rho_{Pt} G_{\uparrow\downarrow} \coth\left(\frac{t_{Pt}}{\lambda_s}\right)}. \quad (3)$$

Similar to the damping increase fitting procedure, we fit the SHMR data in Fig. 4 to Eq. (3) for both the DP mechanism and the

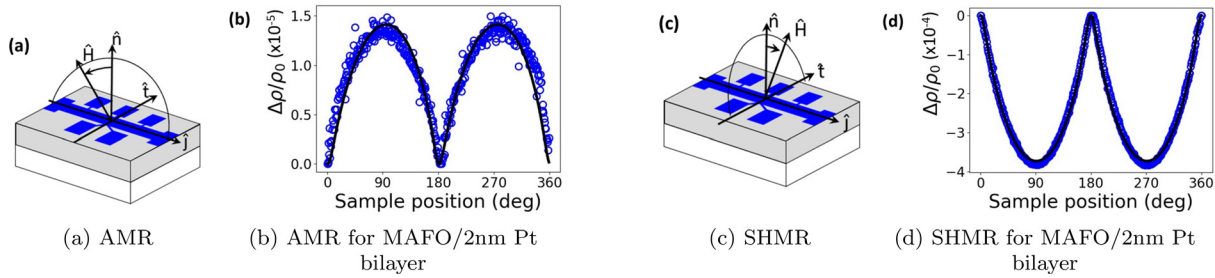


FIG. 3. (a) and (c) Rotation axes to separate contributions from (a) proximity induced magnetism and (c) spin pumping in the metal layer. The external field is along \hat{n} at 0° . (b) The AMR of MAFO/2 nm Pt. (d) The SHMR of MAFO/2 nm Pt. Note the difference in the vertical axis scale for (b) and (d), indicating that AMR is an order of magnitude smaller than SHMR.

EY mechanism. The same thickness dependent resistivity model is used here as in fitting the damping data. We also compare the intrinsic spin Hall effect regime (with θ_{SH} proportional to resistivity) to the extrinsic spin Hall effect regime (where θ_{SH} is constant). We find the SHMR data are best fit by the DP mechanism and an extrinsic spin Hall effect, yielding the values of $G_{\uparrow\downarrow}$ and λ_s consistent with those from the damping data. Thus, in ferrite/Pt bilayers, the DP mechanism is dominant in spin relaxation, and skew scattering is responsible for the spin Hall ratio, indicating a “clean” metal system.¹⁶ Assuming the θ_{SH} of Pt to be between 0.07 and 0.1²⁴ and using the DP extrinsic model, we find $G_{\uparrow\downarrow} = (1.2\text{--}3.5) \times 10^{14} \Omega^{-1} \text{m}^{-2}$ and $\lambda_s = 2.0\text{--}2.3$ nm. These values agree well with those extracted from damping measurements. We note that the DP mechanism and an intrinsic spin Hall effect also appear to fit the SHMR data well (Fig. 4), but the derived spin diffusion length $\lambda_s = 4\text{--}5$ nm is not consistent with that from the damping fit result.

We have demonstrated efficient spin pumping in MAFO/Pt and MAFO/ β -W bilayers with $G_{\uparrow\downarrow}$ around $2 \times 10^{14} \Omega^{-1} \text{m}^{-2}$, which exceeds many reported values for YIG/Pt systems. Spin pumping was detected electrically from the inverse spin Hall effect and through an increase in the Gilbert damping with Pt thickness. We have electrically detected spin currents via the ISHE in Pt and β -W whose opposite spin Hall angles yield opposite voltage signs. In ADMR measurements, we find the SHMR, attributed to spin pumping, to be significantly

larger than the AMR, attributed to proximity-induced magnetism. From the combination of FMR and ADMR measurements, we can determine that the Dyakonov-Perel mechanism and the extrinsic spin Hall effect govern the spin transport in these bilayers, which has not been shown previously in coherently strained spinel-ferrite/Pt systems. These results confirm that this ultralow damping spinel ferrite is an excellent medium for spin current generation, propagation, and control. This opens up possibilities for pure current spintronics based on magnetic insulators.

This work was supported by the Vannevar Bush Faculty Fellowship program sponsored by the Basic Research Office of the Assistant Secretary of Defense for Research and Engineering and funded by the Office of Naval Research through Grant No. N00014-15-1-0045. Part of this work was performed at the Stanford Nano Shared Facilities (SNSF), supported by the National Science Foundation under Award No. ECCS-1542152. The work at the Naval Research Laboratory was supported by a Laboratory University Collaboration Initiative. The work performed at NYU was supported by the National Science Foundation under Award No. NSF-DMR-1610416. S.X.W. was supported in part by Semiconductor Research Corp. and DARPA through the JUMP/ASCENT Center.

REFERENCES

- ¹A. Hoffmann and S. D. Bader, *Phys. Rev. Appl.* **4**, 047001 (2015).
- ²I. Žutić, J. Fabian, and S. D. Sarma, *Rev. Mod. Phys.* **76**, 323 (2004).
- ³M. Onbasli, A. Kehlberger, D. Kim, G. Jakob, M. Kläui, A. Chumak, B. Hillebrands, and C. Ross, *APL Mater.* **2**, 106102 (2014).
- ⁴Z. Qiu, K. Ando, K. Uchida, Y. Kajiwara, R. Takahashi, H. Nakayama, T. An, Y. Fujikawa, and E. Saitoh, *Appl. Phys. Lett.* **103**, 092404 (2013).
- ⁵H. Wang, C. Du, Y. Pu, R. Adur, P. C. Hammel, and F. Yang, *Phys. Rev. Lett.* **112**, 197201 (2014).
- ⁶J. Lustikova, Y. Shiomi, Z. Qiu, T. Kikkawa, R. Iguchi, K. Uchida, and E. Saitoh, *J. Appl. Phys.* **116**, 153902 (2014).
- ⁷B. Howe, S. Emori, H. Jeon, T. Oxholm, J. Jones, K. Mahalingam, Y. Zhuang, N. Sun, and G. Brown, *IEEE Magn. Lett.* **6**, 3500504 (2015).
- ⁸S. Yoon, C. Vittoria, and S. Oliver, *J. Appl. Phys.* **93**, 4023 (2003).
- ⁹P. Li, T. Liu, H. Chang, A. Kalitsov, W. Zhang, G. Csaba, W. Li, D. Richardson, A. DeMann, G. Rimal *et al.*, *Nat. Commun.* **7**, 12688 (2016).
- ¹⁰S. Emori, B. A. Gray, H.-M. Jeon, J. Peoples, M. Schmitt, K. Mahalingam, M. Hill, M. E. McConney, M. T. Gray, U. S. Alaan *et al.*, *Adv. Mater.* **29**, 1701130 (2017).
- ¹¹S. Emori, D. Yi, S. Crossley, J. J. Wissner, P. P. Balakrishnan, B. Khodadadi, P. Shafer, C. Klewe, A. T. N'Diaye, B. T. Urwin *et al.*, *Nano Lett.* **18**(7), 4273–4278 (2018).
- ¹²M. Gray, S. Emori, B. Gray, H. Jeon, O. van't Erve, B. Jonker, S. Kim, M. Suzuki, T. Ono, B. Howe *et al.*, *Phys. Rev. Appl.* **9**, 064039 (2018).

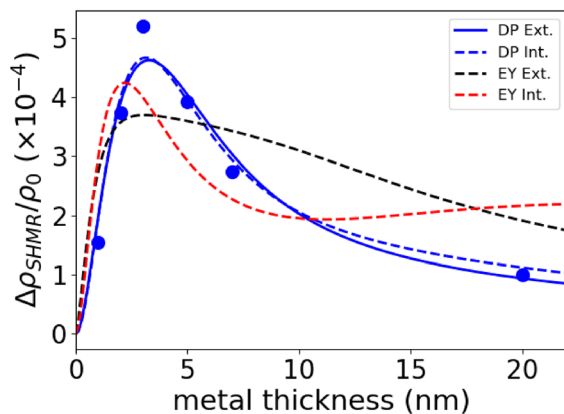


FIG. 4. SHMR ratio at 2 T for different Pt thicknesses. The data are fit to Eq. (3) for the Dyakonov-Perel mechanism and the Elliott-Yafet mechanism, as well as the extrinsic and intrinsic spin Hall effects.

- ¹³L. Kang, J. Gao, H. Xu, S. Zhao, H. Chen, and P. Wu, *J. Cryst. Growth* **297**, 100 (2006).
- ¹⁴M. P. Warusawithana, C. Cen, C. R. Sleasman, J. C. Woicik, Y. Li, L. F. Kourkoutis, J. A. Klug, H. Li, P. Ryan, L.-P. Wang *et al.*, *Science* **324**, 367 (2009).
- ¹⁵L. Ma, L. Lang, J. Kim, Z. Yuan, R. Wu, S. Zhou, and X. Qiu, *Phys. Rev. B* **98**, 224424 (2018).
- ¹⁶E. Sagasta, Y. Omori, M. Isasa, M. Gradhand, L. E. Hueso, Y. Niimi, Y. Otani, and F. Casanova, *Phys. Rev. B* **94**, 060412 (2016).
- ¹⁷L. Liu, R. Buhrman, and D. Ralph, "Review and Analysis of Measurements of the Spin Hall Effect in Platinum," preprint [arXiv:1111.3702](https://arxiv.org/abs/1111.3702) (2011).
- ¹⁸E. Saitoh, M. Ueda, H. Miyajima, and G. Tatara, *Appl. Phys. Lett.* **88**, 182509 (2006).
- ¹⁹D. Meier, D. Reinhardt, M. Van Straaten, C. Klewe, M. Althammer, M. Schreier, S. T. Goennenwein, A. Gupta, M. Schmid, C. H. Back *et al.*, *Nat. Commun.* **6**, 8211 (2015).
- ²⁰F. Wilhelm, P. Pouloupoulos, G. Ceballos, H. Wende, K. Baberschke, P. Srivastava, D. Benea, H. Ebert, M. Angelakeris, N. Flevaris *et al.*, *Phys. Rev. Lett.* **85**, 413 (2000).
- ²¹S.-Y. Huang, X. Fan, D. Qu, Y. Chen, W. Wang, J. Wu, T. Chen, J. Xiao, and C. Chien, *Phys. Rev. Lett.* **109**, 107204 (2012).
- ²²Z. Feng, J. Hu, L. Sun, B. You, D. Wu, J. Du, W. Zhang, A. Hu, Y. Yang, D. Tang *et al.*, *Phys. Rev. B* **85**, 214423 (2012).
- ²³C. Hahn, G. De Loubens, O. Klein, M. Viret, V. V. Naletov, and J. B. Youssef, *Phys. Rev. B* **87**, 174417 (2013).
- ²⁴M. Weiler, G. Woltersdorf, M. Althammer, H. Huebl, and S. T. Goennenwein, *Solid State Physics* (Elsevier, 2013), Vol. 64, pp. 123–156.
- ²⁵B. Heinrich, *Ultrathin Magnetic Structures III* (Springer, 2005), pp. 143–210.
- ²⁶Y. Tserkovnyak, A. Brataas, and G. E. Bauer, *Phys. Rev. B* **66**, 224403 (2002).
- ²⁷C. T. Boone, H. T. Nembach, J. M. Shaw, and T. J. Silva, *J. Appl. Phys.* **113**, 153906 (2013).
- ²⁸V. Castel, N. Vlietstra, J. Ben Youssef, and B. J. van Wees, *Appl. Phys. Lett.* **101**, 132414 (2012).
- ²⁹M. Haertinger, C. Back, J. Lotze, M. Weiler, S. Geprägs, H. Huebl, S. Goennenwein, and G. Woltersdorf, *Phys. Rev. B* **92**, 054437 (2015).
- ³⁰J.-C. Rojas-Sánchez, N. Reyren, P. Laczkowski, W. Savero, J.-P. Attané, C. Deranlot, M. Jamet, J.-M. George, L. Vila, and H. Jaffrès, *Phys. Rev. Lett.* **112**, 106602 (2014).
- ³¹S. Emori, A. Matyushov, H.-M. Jeon, C. J. Babroski, T. Nan, A. M. Belkessam, J. G. Jones, M. E. McConney, G. J. Brown, B. M. Howe *et al.*, *Appl. Phys. Lett.* **112**, 182406 (2018).
- ³²Y. Sun and M. Wu, *Solid State Physics* (Elsevier, 2013), Vol. 64, pp. 157–191.
- ³³M. M. Qaid, T. Richter, A. Müller, C. Hauser, C. Ballani, and G. Schmidt, *Phys. Rev. B* **96**, 184405 (2017).
- ³⁴H. Nakayama, M. Althammer, Y.-T. Chen, K. Uchida, Y. Kajiwara, D. Kikuchi, T. Ohtani, S. Geprägs, M. Opel, S. Takahashi *et al.*, *Phys. Rev. Lett.* **110**, 206601 (2013).
- ³⁵M. Althammer, S. Meyer, H. Nakayama, M. Schreier, S. Altmannshofer, M. Weiler, H. Huebl, S. Geprägs, M. Opel, R. Gross *et al.*, *Phys. Rev. B* **87**, 224401 (2013).
- ³⁶S. Vélez, V. N. Golovach, A. Bedoya-Pinto, M. Isasa, E. Sagasta, M. Abadia, C. Rogero, L. E. Hueso, F. S. Bergeret, and F. Casanova, *Phys. Rev. Lett.* **116**, 016603 (2016).
- ³⁷Y.-T. Chen, S. Takahashi, H. Nakayama, M. Althammer, S. T. Goennenwein, E. Saitoh, and G. E. Bauer, *Phys. Rev. B* **87**, 144411 (2013).